ChemistrySelect

Research Article
doi.org/10.1002/slct.202400838

Chemistry Europe
European Chemical Societies Publishing

www.chemistryselect.org

A Flexible Reduced Graphene Oxide-based Paper for Supercapattery Design: Effect of Polyindole Thin Films and Zinc Oxide Nanoparticles

Esra Atalay Mollamehmetoğlu[a] and Murat Alanyalıoğlu*[a, b]

Flexible graphene-based paper electrodes (FGPEs) are a new class of study and the research on this electrode material has been carried out for approximately ten years. FGPEs have many advantages compared to classical solid electrodes such as being flexible, foldable, adaptable to flexible electronics, being cut, easily shaped, and effective and adjustable modification. In this work, the applicability of FGPEs modified with polyindole (PIN) thin films and zinc oxide nanoparticles (ZnO-NPs) to energy-storage systems as a supercapattery design is presented, and especially the limitations of ZnO-NPs for energy-storage applications are revealed to inform researchers working for a similar purpose. Capacitance calculations have been performed using both cyclic voltammetry (CV) and galvanostatic charge-discharge (GCD) experiments. It was observed that the rGO/PIN paper demonstrated almost 30 times more energy-storage capacity than that of the rGO/PIN/ZnO paper due to the electrochemical instability of ZnO-NPs on the flexible electrode platform at the applied potential region in 1.0 M $HClO_4$ solution. The rGO/PIN paper with a highly flexible property exhibited an energy density of 74.5 $W h cm^{-2}$ and a power density of 2258 $W cm^{-2}$ at a current density of 2.2 $mA cm^{-2}$, revealing hopeful results for future modular and flexible approaches.

Introduction

Energy storage systems accumulate energy in the electrochemical, chemical, kinetics, pressure, potential, electromagnetic, or thermal forms. Supercapacitors are the most interesting among energy storage devices due to their high power density, rapid charge-discharge property, long-term usage, and environmentally friendliness. Different strategies are carried out in the development of materials that can provide advantages for supercapacitors. In such studies, the advantages of pseudocapacitors by using polymers and metal oxide nanoparticles as well as carbon nanomaterials such as graphene, carbon nanotube, and fullerene to use the characteristics of electric double layer capacitors (EDLCs) for electrode design are reflected till now.[1,2] In this field, two different studies are performed. Traditional supercapacitor designs contain non-flexible traditional electrodes such as Au wire,[1] Ni wire,[2] pencil graphite,[3] and glassy carbon.[4] In such studies, the composite structure is usually covered directly on these solid substrates using an appropriate method such as drop-casting. The second type of application includes flexible and wearable supercapacitor designs. A flexible character can be achieved by two approaches: coating capacitive material onto a flexible substrate[5–8] or production of capacitive flexible paper-like materials.[9,10] Due to the advantages of simple adjustment of paper thickness, easy arrangement of chemical composition, high flexibility, durable structure, and integration to wearable applications, it is noteworthy that more research has been conducted on the production of flexible graphene-based paper electrodes (FGPEs) for various electrochemical applications e.g. supercapacitors,[10] batteries,[11] and electrochemical sensors.[12–14] These paper-like electrodes can be created using different methods such as mold casting,[10] vacuum-filtration,[14,15] bar-coating,[16] inkjet-printing,[17] and pressing.[18]

A new energy-storage idea was put forward in 2009 by Klumpner et al.,[19] consisting of a high power density of EDLC on one side and a high energy density of battery-type electrodes on the other side. This design has been called a supercapattery because this hybrid structure is a combination of supercapacitors and batteries. In this asymmetric composition, battery-type materials are used as the positive electrode and carbon-based materials with EDLC character are used as the negative electrode,[19–21] In the literature, free-standing supercapatteries are mainly produced by modification of nickel foam,[22–24] aerogel,[25] and carbon fabric[26–28] substrates. It is noteworthy that the use of FGPEs in supercapattery design is very limited in the literature and no significant study has been published in this field. Polyindole (PIN) films[1,2,29–32] and zinc oxide nanoparticles (ZnO-NPs)[7,33] have been studied for energy-storage systems because contribution as redox-active and electron mediator role with a highly conjugated structure of PIN films and capacitive properties of semiconductor ZnO-NPs. As illustrated in Figure 1, indole has an integrated aromatic structure and PIN shows a lower hydrolytic degradation than other polymers such as polyaniline. PIN has a competitive redox potential with polypyrole and its charged or discharged phase does not involve any salt formation.[32] ZnO-NPs is a semi-

[a] E. A. Mollamehmetoğlu, M. Alanyalıoğlu
Sciences Faculty, Department of Chemistry, Atatürk University, 25240 Erzurum, Türkiye

[b] M. Alanyalıoğlu
Vocational School, Department of Food Processing, Bilecik Şeyh Edebali University, Bilecik, Türkiye
E-mail: murat.alanyalioglu@bilecik.edu.tr

Supporting information for this article is available on the WWW under https://doi.org/10.1002/slct.202400838

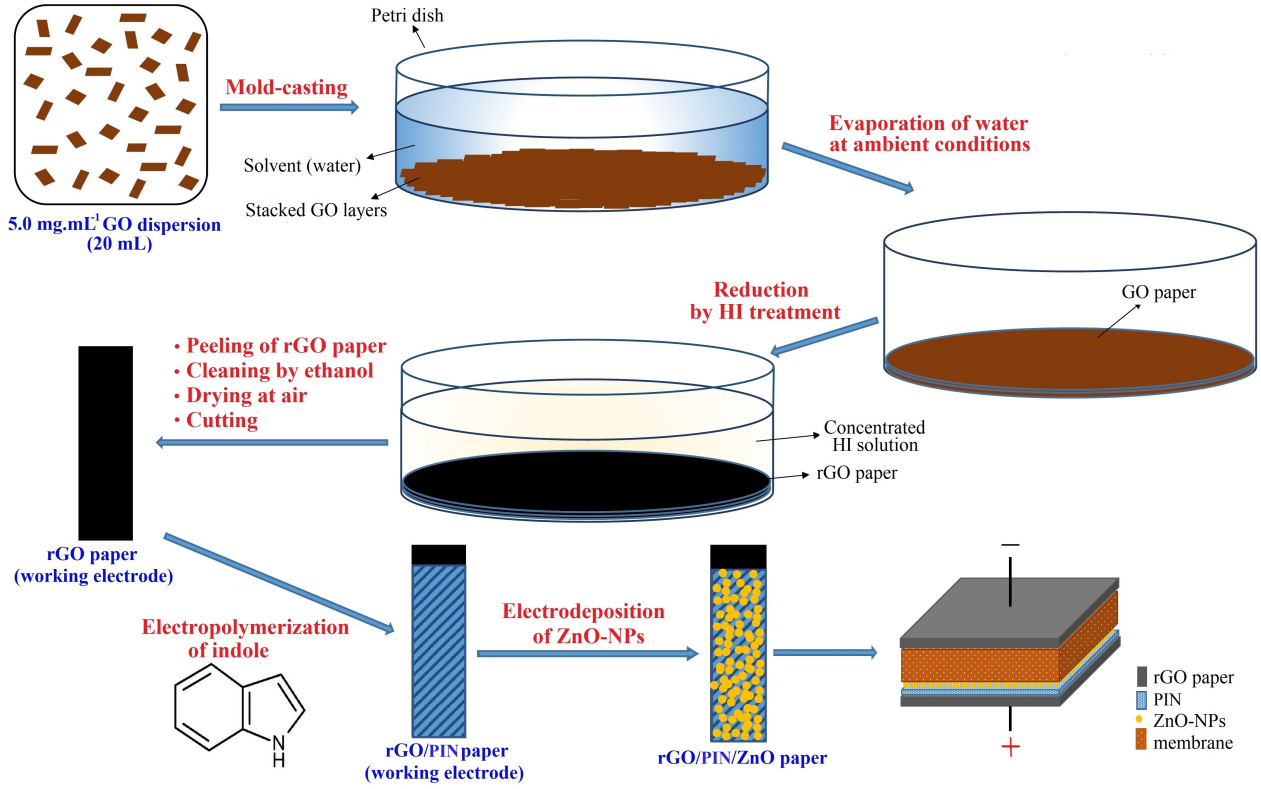

Figure 1. Experimental detail of preparation of rGO/PIN/ZnO paper for supercapattery application.

conductor material, with a direct band gap value of 3.3 eV and it is preferred in energy-storage devices due to its high energy density of 650 A g^{-1}.[33]

The study aims to investigate the usability of FGPEs as a flexible and durable platform in supercapattery production and to evaluate the contribution of PIN thin films and ZnO-NPs for the energy-storage performance as well as reveal a detailed characterization for performed electrochemical modifications on flexible rGO papers. For this purpose, graphene oxide (GO) paper was initially prepared by mold-casting of GO dispersion. The GO paper was treated with HI to prepare reduced graphene oxide (rGO) paper because rGO paper is electrochemically conductive and electroactive. The rGO paper was modified with PIN thin films performing potentiodynamic or potentiostatic approaches in electrochemical cells including indole, and then ZnO-NPs were immobilized onto rGO/PIN paper by one-pot electrodeposition route. Characterization of rGO, rGO/PIN, and rGO/PIN/ZnO paper samples was carried out using numerous techniques, and specific capacitance (C_s) measurements were applied using both cyclic voltammetry (CV) and galvanostatic charge-discharge (GCD) experiments.

Experimental Section

Preparation of rGO Paper

All of the chemicals have been used as purchased without further purification. Graphite oxide powder was produced by a chemical oxidation process using a modified Hummers method following our previous study.[14] After synthesis, 5.0 mg mL^{-1} aqueous dispersion of GO was prepared by dispersing a certain amount of graphite oxide under ultrasonic treatment for 6 h using Bandelin Sonorex ultrasonic bath. A mold-casting method was employed to obtain flexible and free-standing rGO paper. 20 mL of the prepared 5.0 mg mL^{-1} GO dispersion was transferred to a Petri container and kept until the solvent (deionized water) was away from room temperature. 10 mL of concentrated HI was added, kept overnight, and then removed from the Petri mold. The obtained free-standing rGO paper was cleaned with ethanol to remove residue HI from the paper, and dried at the atmospheric conditions (Figures 1 and S1).

Preparation of rGO/PIN Paper

To modify rGO paper with PIN thin films, electropolymerization of indole has been performed using repetitive CV application in 0.10 M $HClO_4$ solution containing 1.0 mM indole. For this purpose, an rGO paper electrode, a Pt wire, and an Ag/AgCl (sat. KCl) were served as working, counter, and reference electrodes, respectively. Alternatively, controlled potential electrolysis (CPE) was also applied for electropolymerization of indole.

Production of rGO/PIN/ZnO and rGO/ZnO Papers

Modification of ZnO nanoparticles has been achieved using by CPE technique following the literature study.[34] Accordingly, rGO/PIN paper was used as a working electrode in 0.10 M $Zn(NO_3)_2$ solution (pH: 5.0) at the constant temperature of 80 °C using a thermostatic cell. The rGO/ZnO paper production was also provided by performing the same approach on the rGO paper electrode.

Instrumentation

Optical information on the samples was acquired using Shimadzu brand UV-Vis. Spectrophotometer and Perkin-Elmer Spectrum One Fourier-Transform Infrared (FTIR) spectrometer with specular reflectance accessory. Morphological characterization was performed using scanning tunnel microscopy (STM) (Molecular Imaging brand) and scanning electron electron microscopy (SEM) (FEI Inspect). Crystal structure analysis was executed using the Rigaku brand miniflex model powder XRD device (Cu Kα, λ = 1.54 Å). Raman spectrometer (WITech alpha 300 R) and X-ray photoelectron spectrometer (XPS) (Specs-Flex) were also applied to obtain structural information about paper samples. CV, CPE, GCD, and electrochemical impedance spectroscopy (EIS) were implemented with the Gamry brand potentiostat system. Electrode surface area was calculated based on the Randles-Sevcik equation using related CV data (See supplementary information).

Supercapattery Performance

To reveal the supercapattery performances, not only a three-electrode cell was constituted but also a two-electrode cell as rGO/PIN//rGO was also created and optimization of important parameters, reproducibility, and flexibility were questioned by calculating the C_s, energy density, power density, and efficiency values of the prepared paper electrodes (See supplementary information)

Results and Discussion

Electropolymerization of Indole on rGO Paper

First of all, the quality of GO sheets is a very important issue for the performance of FGPEs. For the characterization of produced GO sheets, optical, crystallographic, and morphological analyses have been performed. UV-Vis. absorption spectrum of GO dispersion (Figure S2a) shows a band at 232 nm with a shoulder at 300 nm, associated with π-π transitions of C=C bonds and n-π transitions of oxygenated groups, respectively.[35] A strong peak at 2θ = 10.9° in the XRD pattern confirms the formation of GO layers and a broad band with a very low intensity at around 2θ = 21.0° reveals that there may be a few-layered GO structure with a very low amount (ICDD-PDF #411487) (Figure S2b).[36] The STM image taken for rGO layers on Au(111) substrate demonstrates a surface structure covered in flat foils with approximately 150–300 nm size and 0.3 nm thickness, corresponding to an atomic layer (Figure S2c).

The PIN layers were immobilized onto rGO paper using both repetitive scan of CV and constant potential approach with CPE. The 50 consecutive CVs of rGO paper in 0.10 M $HClO_4$ solution containing 1.0 mM indole are seen in Figure S3. A peak pair at around +600/+400 mV emerges after the first scan and the current of this peak pair increases with the number of cycles, indicating the formation of PIN film on the rGO paper.[37] As the aim of this study is to produce an effective energy storage device, fabrication conditions of PIN thin film need to be optimized based on the highest C_s value. First of all electrolyte type is the most important issue and it is obvious that acidic medium (1.0 M $HClO_4$ solution) exhibits the highest C_s value of 24.7 mF cm^{-2} when compared to neutral (1.0 M Na_2SO_4) and basic (1.0 M KOH) electrolyte solutions (Figure 2).

Figure 3a represents the repetitive CVs for electropolymerization of indole on rGO paper working electrode, by reversing from different upper potential limits. If potential cycling is applied from +800 mV, the peak pair of PIN is hardly seen due to inadequate oxidation, while the redox pair at about +600/+400 mV arises after +900 mV, and the current density of these peaks increases for +1000 mV. After the upper potential limit of +1100 mV, a dramatic decrease in current density of PIN redox peaks indicates over-oxidation of polymeric film. Hence, the highest current density of PIN redox pair is obtained for the upper potential limit of +1000 mV and this case is confirmed by CV of this rGO/PIN paper in 1.0 M $HClO_4$ solution, which presents a C_s value of 31.7 mF cm^{-2} a seen in Figure 3b. Figure 3c illustrates that the polymeric film thickness increases by number of CV cycling and C_s value rises till 50 cycles but then reduces for 100 and 150 cycles. The electrical conductivity of rGO paper and PIN films have previously been measured as 1.08×10^4 and 9.64×10^{-1} S m^{-1}, respectively[14,38] and the diminish in the electrical conductivity can be associated with the decrease in the conductivity of the electrode by the increase of PIN film thickness.

An alternative method for electropolymerization is CPE and current density-time transients of different electrooxidation potentials for 15 min are represented in Figure 4a. The current density value decreases exponentially by the time starting from a maximum value, indicating the Langmuir-type electrodeposi-

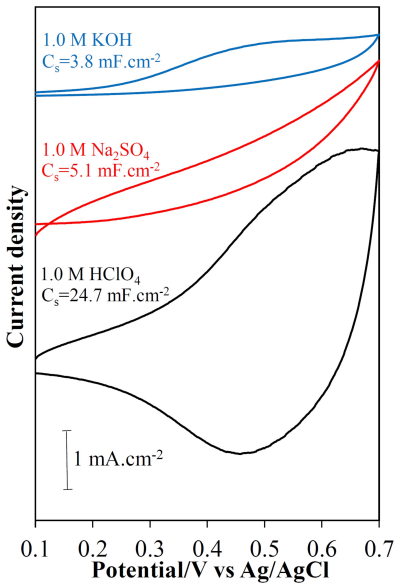

Figure 2. CVs and calculated C_s values of rGO/PIN paper in various electrolyte solutions. Scan rate: 50 mV s^{-1}.

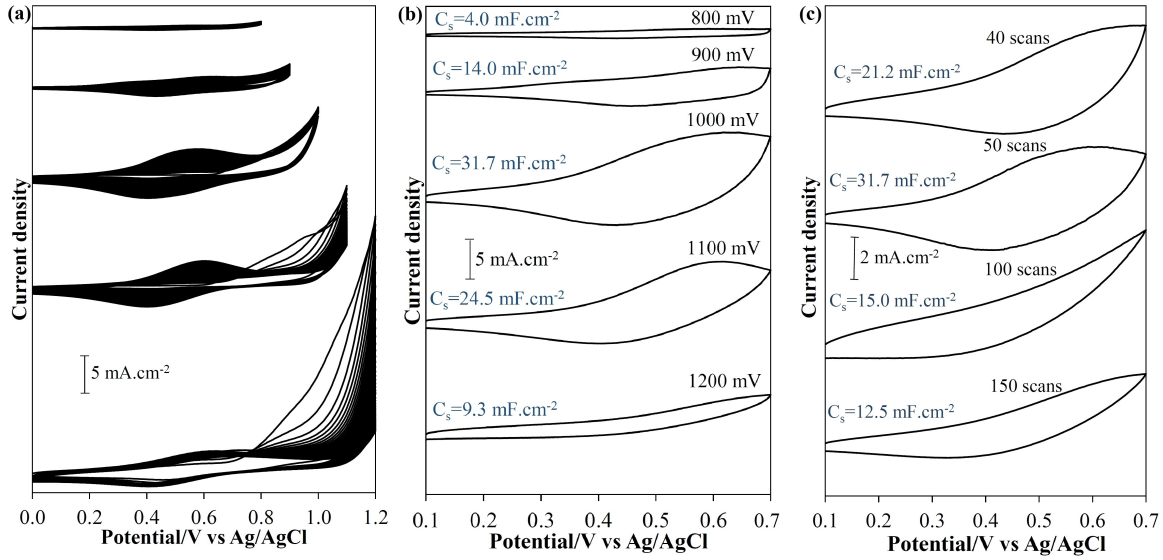

Figure 3. Electropolymerization of indole in 0.10 M $HClO_4$ solution containing 1.0 mM indole on rGO paper at different upper potential limits (a). CVs of rGO/PIN papers prepared at different upper potential limits in 1.0 M $HClO_4$ solution (b). CVs of rGO/PIN paper prepared at +1000 mV for different cycling numbers (c). Scan rate: 50 mV s^{-1}.

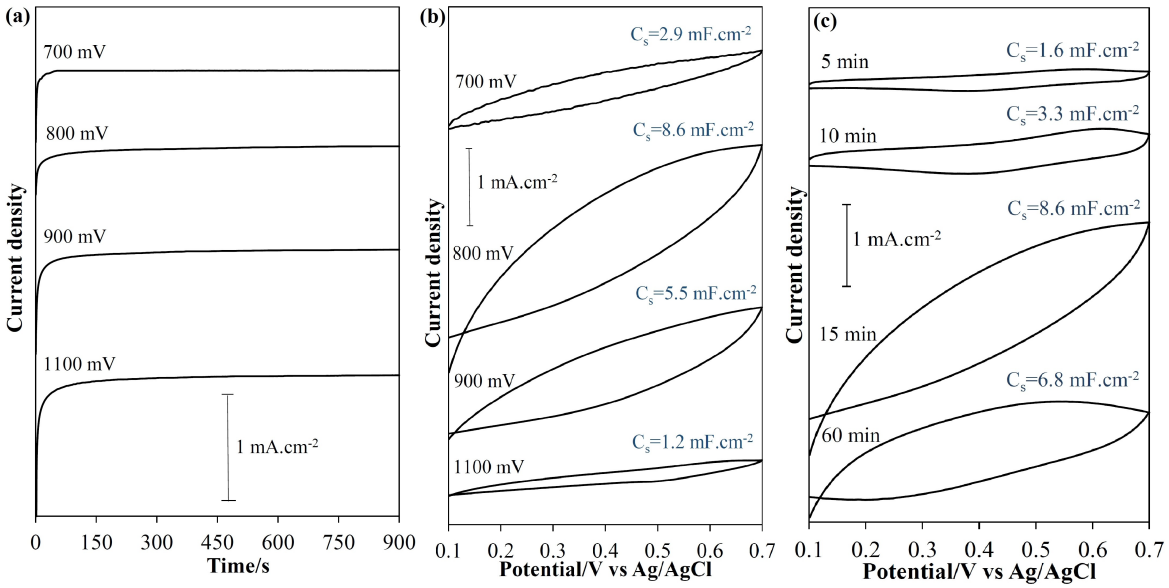

Figure 4. CPE data of rGO paper in 0.10 M $HClO_4$ solution containing 1.0 mM indole applied at different electrooxidation potentials for 15 min (a). CVs of rGO/PIN papers prepared at different electrooxidation potentials in 1.0 M $HClO_4$ solution (b). CVs of rGO/PIN paper prepared at +800 mV for different times (c). Scan rate: 50 mV s^{-1}.

tion process.[39] According to the CVs taken in 1.0 M $HClO_4$ solution to determine the C_s values of each rGO/PIN paper prepared in this way, the highest value was obtained as 8.6 mF cm^{-2} for the paper prepared at +800 mV for 15 min (Figure 4b and c). This current density is about 1/4 of the C_s value of the rGO/PIN paper prepared with successive CV application.

Electrodeposition of ZnO-NPs on rGO and rGO/PIN papers

The powder XRD data for rGO and rGO/PIN paper are presented in Figure S4. In the XRD pattern of rGO paper, a severe peak appears at $2\theta = 23.5°$, corresponding to the distance between the layers (d) of 0.38 nm. The d value for pure graphite is 0.34 nm (ICDD-PDF #411487). It can be deduced oxidation and reduction process for the production of rGO paper results in a higher d value than graphite due to the partial reduction of GO paper by HI treatment. It is noteworthy that the XRD data of the

rGO/PIN paper is almost the same as the rGO paper, which indicates the amorphous structure of PIN thin films.

Fabrication of rGO/ZnO paper has been achieved by a simple electrodeposition in 0.10 M $Zn(NO_3)_2$ solution (pH: 5.0) at 80 °C. For this purpose, electrodeposition potential and time were initially optimized as seen in Figure 5. CV data for different cycling potentials show that the reduction of Zn^{2+} species occurs at negative potentials than −600 mV. However, the formation of hydrogen gas is accompanied the deposition of Zn film at around −1000 mV.

The effect of electrodeposition potential is displayed in Figure 5b. A peak originated at 2θ of 23.5° formed in all XRD patterns corresponds to rGO layers[40,41] by taking XRD data of rGO paper (Figure S4) account. The peaks at 2θ of 31.1, 33.4, 35.3, 46.4, 55.7, 62.0, 67.2, 71.8 and 75.8° can be assigned to 100, 002, 101, 102, 110, 103, 200, 004 and 202 orientation of ZnO-NPs, respectively (JCPDS No: 36-1451).[41] Considering the intensities of the ZnO peaks, the optimum electrooxidation potential was selected as −700 mV. Based on the same criteria, the best electrodepositon time can be elected as 30 min as seen in Figure 5c. Since our main aim is to prepare rGO/PIN/ZnO papers, electrodeposition of ZnO was applied on rGO/PIN paper at different electrodeposition potentials and durations as illustrated in Figure 6. It is clear that most preferably electrodeposition conditions are −800 mV (Figure 6a) for 30 min (Figure 6b) taking the intensity of the the peaks for formation of ZnO thin films on rGO/PIN paper.

Characterization of FGPEs

Different techniques have been used for the characterization of all fabricated paper-like materials. FTIR results are demonstrated in Figure 7a. It is noteworthy that the severe -OH band at 3375 cm^{-1} observed for GO paper has a significant decrease by the reduction process. The contribution of both ZnO-NPs and PIN films to rGO paper makes a significant increase in the intensity of –OH band. The attachment of PIN films for both rGO/PIN and rGO/PIN-ZnO papers reveals an intensive peak at 2940 cm^{-1} corresponding to C–H stretching mode and a shoulder at 3280 cm^{-1} due to N–H stretching vibration of aromatic indole structure.[42–44]

Raman spectroscopy was used to get further structural information (Figure 7b and c). It is seen that D and G bands are formed at 1344 and 1584 cm^{-1} values for rGO paper at λ_{ex} = 785 nm. The D band takes place in defective graphene structures and the G band is the vibration mode that occurs for C=C bond of graphene flakes.[45] The rGO/PIN and rGO/PIN/ZnO papers also contain D and G bands with new weak peaks at around 1000–1500 cm^{-1} corresponding to PIN films at λ_{ex} = 785 nm (Figure 7b).[43,46] To verify the peaks of PIN films, Raman spectra of both rGO/PIN and rGO/PIN/ZnO papers have been obtained at λ_{ex} = 532 nm. It is seen that peaks of PIN thin films get intensive in the region of 1000–1500 cm^{-1}, with the formation of a broad band at approximately 3000 cm^{-1} (Figure 7c). It is noteworthy that with excitation at 532 nm not only the broad band at around 3000 cm^{-1} arises but also the structure of the entire spectrum changes and the baseline shows a rise through high wavenumbers. The presence of the broad band for λ_{ex} = 532 nm may be due to the fluorescence of deposited PIN thin films on rGO paper.[46]

The intensity ratio of the D to G band is related to the defect density of FGPEs[37] and I_D/I_G values were calculated as 1.44, 1.33, 1.30, and 1.52 for rGO, rGO/ZnO, rGO/PIN, and rGO/PIN/ZnO paper samples, respectively. It can be deduced that the defect density decreases with the contribution of ZnO-NPs to rGO paper and the inclusion of PIN results in the lowest I_D/I_G value, which can be associated with a patch role of various

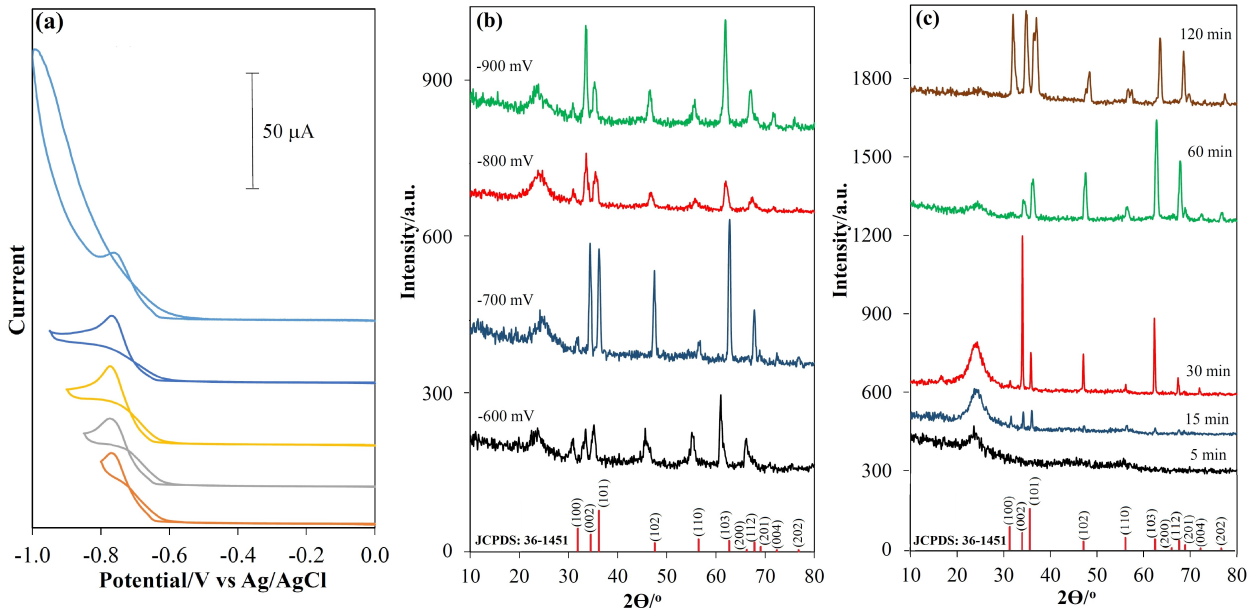

Figure 5. CVs of rGO paper in 0.10 M $Zn(NO_3)_2$ (pH: 5.0) solution at 80 °C. Scan rate: 50 mV s^{-1} (a). XRD patterns of rGO/ZnO papers prepared at different potentials for 30 min (b) and prepared at −700 mV for different deposition times.

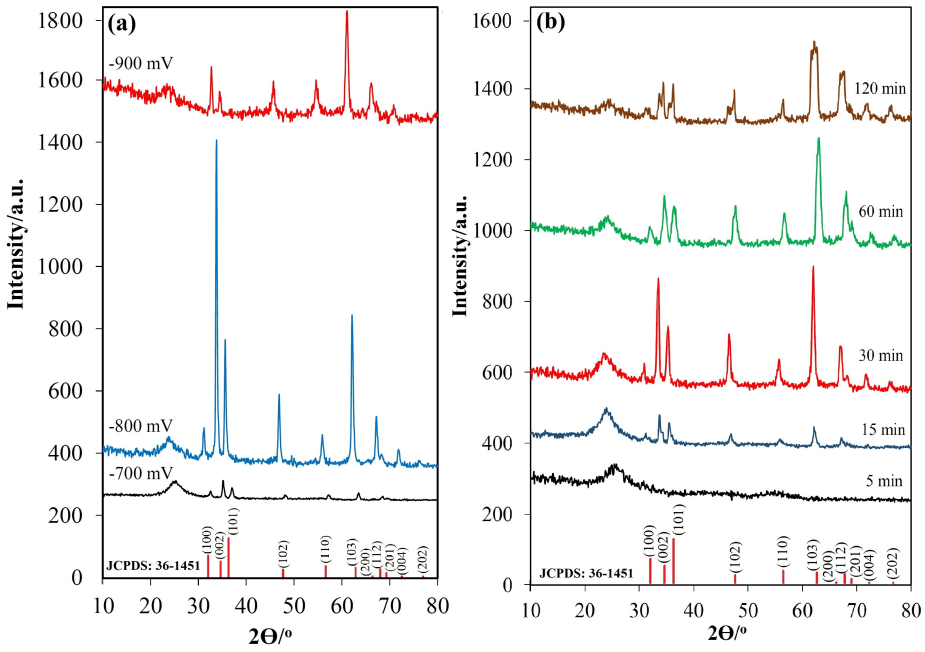

Figure 6. XRD patterns of rGO/PIN/ZnO papers prepared at different potentials for 30 min (a) and prepared at −800 mV for different times in 0.10 M $Zn(NO_3)_2$ solution (pH: 5.0) (b).

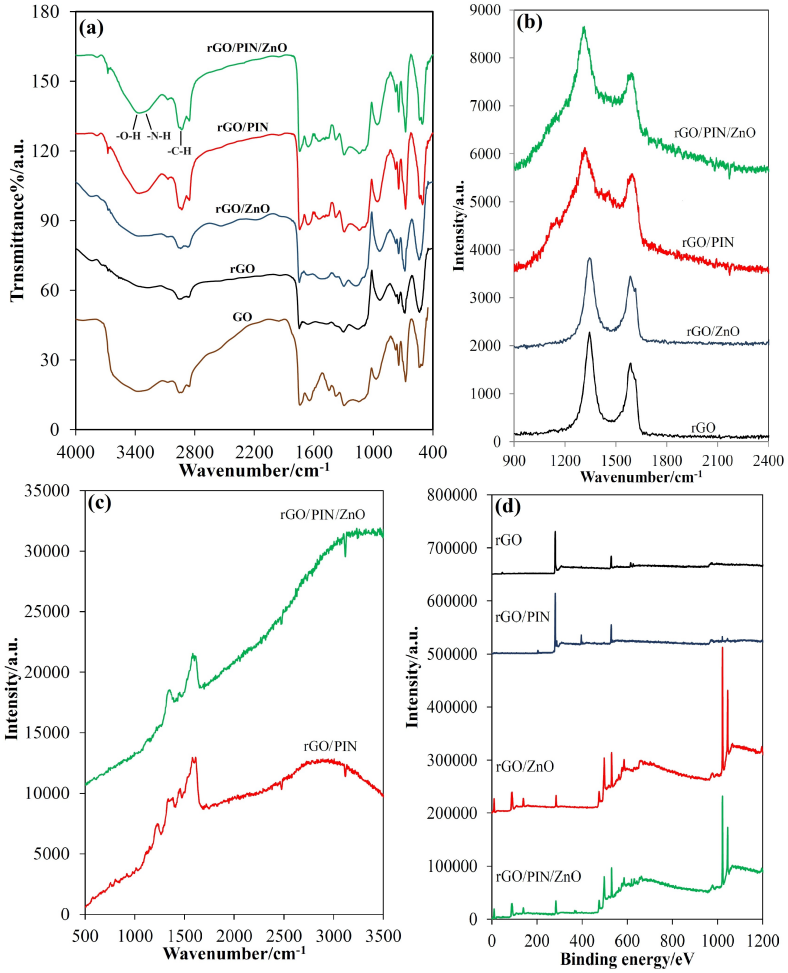

Figure 7. FTIR (a), Raman (b, c), and XPS (d) data of various paper-like samples. λ_{ex} are 785 and 532 nm for b and c, respectively.

materials on the defects of the graphene sheets. The highest defect density was obtained in rGO/PIN/ZnO paper, indicating the formation of two different layers on rGO paper causes a more flawed structure than on rGO paper.

Elemental analysis was executed using the XPS technique (Figure 7d). As summarized in Table S1, the rGO paper sample includes 86.77% C and 10.59% O, presenting a C/O ratio of 8.19. In our previous study, the C/O ratio for GO and rGO papers has been reported as 2.79 and 7.49, respectively.[36] The presence of 0.61% iodine states a low amount of residual HI from the reduction process. It is estimated that the low content of nitrogen in the rGO paper structure is caused by air. XPS results indicate immobilization of both PIN and ZnO-NPs onto rGO paper with the presence of 7.79% nitrogen in rGO/PIN paper and 23.5% of Zn atom in rGO/ZnO paper. It should also be noted that the oxygen amount increases after the electrodeposition of ZnO-NPs onto rGO paper. In rGO/PIN/ZnO paper, the existence of nitrogen, zinc, and a relatively high amount of oxygen is remarkable. It is thought that the cause of low-content foreign atoms arises from contamination during the XPS analysis.

Surface and cross-sectional SEM analysis was executed to obtain morphological information of the FGPEs. Figures 8a and S5a exhibit that rGO paper has a homogeneous structure and a higher magnification SEM image (Figure S6a) indicates that the surface of rGO paper contains wrinkled shapes. The rGO/PIN paper also displays a curved surface structure with additional nanoparticles with 100–200 nm size on rGO paper (Figures 8b, S5b, and S6b). Electrodeposition of ZnO-NPs on rGO paper shows a dense flower-like deposit, in which the curved view is disappeared (Figures 8c, S5c, and S6c). For the electrodeposition of ZnO-NPs, it is supposed that the crumpled surface of rGO paper plays a template role for nucleation and growth of flower-like crystals.[47] When ZnO-NPs are modified onto rGO/PIN paper, the surface is covered with crystals in relatively larger circular/oval particles with a lower surface density (Figure 8d). When we focus on this SEM image, the presence of spherical ZnO crystals is observed with size varying between 2 and 8 μm (Figure S5d), in which flower-like sub-crystals formed (Figure S6d). It is supposed that the formation of ZnO crystals began around the interlayer PIN nanoparticles rather than wrinkled rGO paper and resulted in larger particles with lower surface coverage.

To investigate lateral change on rGO paper after electrochemical modifications, cross-sectional SEM analysis was performed as shown in Figure 8. The rGO paper with approximately 3 μm thickness exhibits a layered and highly stacked lateral view (Figure 8a). The regularly-layered structure of rGO paper is not preserved after electropolymerization of indole, which is associated with coverage of PIN films between rGO layers besides surface immobilization. (Figure 8b). After electrodeposition of ZnO-NPs on rGO paper, both surfaces of rGO paper consist of highly-packed ZnO films with around 2 μm thickness (Figure 8c). It is noteworthy that ZnO-NPs are not electrodeposited between the rGO layers. The rGO/PIN/ZnO paper exhibits a hybrid view of rGO/PIN and rGO/ZnO cross-sectional SEM images, in which regular rGO layers are destroyed by electropolymerization of indole and ZnO-NPs are hardly visible due to lower coverage of ZnO-NPs onto rGO/PIN paper (Figure 8d).

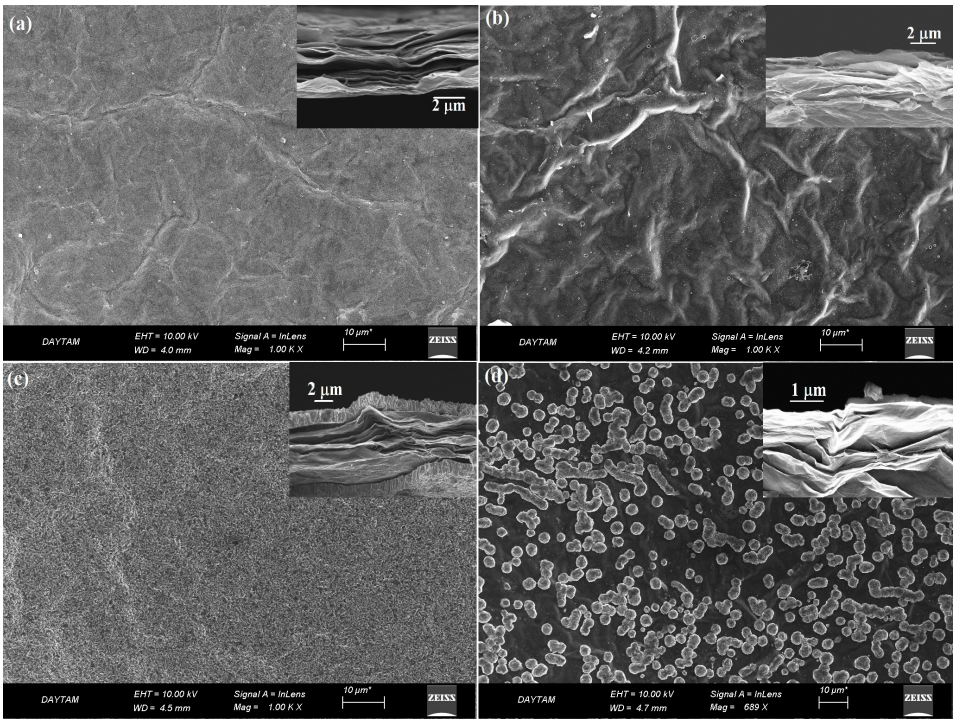

Figure 8. SEM images of rGO (a), rGO/PIN (b), rGO/ZnO (c), and rGO/PIN/ZnO (d) papers. Insets: Cross-sectional views or related paper-like samples.

Supercapattery Studies

The most suitable potential window of rGO/PIN paper in 1.0 M $HClO_4$ solution for energy storage applications is seen as 0.1 to 0.7 V considering the redox behavior of PIN films as represented in Figures 2 and S3. When the electrochemical behavior of the rGO/PIN/ZnO paper in this potential range is examined, it is observed that the ZnO thin film is unstable due to stripping from the rGO paper surface (Figure S7a). For this case, the following electrochemical stripping route can be suggested for the dissolution of ZnO-NPs from the electrode surface.[48]

$$ZnO(s) \rightarrow Zn^{2+} + {}^{1}/_{2}O_2 + 2e^- \quad (1)$$

It is also known that ZnO is chemically dissolved in an aqueous medium based on the following reaction and the dissolution rate increases with the increment of acidity of the solution and treatment time.[49]

$$ZnO(s) + 2H^+ \rightarrow Zn^{2+} + H_2O \quad (2)$$

To understand this case clearly, CV data of rGO/PIN paper in the potential range of 0.1–0.7 V for 7 consecutive scans was acquired in 1.0 M $HClO_4$ solution (Figure S7b), in which a stable rGO/PIN paper is remarkable but this potential window is not suitable for rGO/PIN/ZnO paper for energy storage approaches. A detailed potential scan was performed to determine a suitable potential range of rGO/PIN/ZnO paper for the supercapattery design. Figure S7c shows CVs of rGO/PIN/ZnO paper scanned from various positive and negative potential limits. Based on this CV data, potential scale of −0.1 and 0.2 V was evaluated as suitable for rGO/PIN/ZnO paper but testing this potential windows with 7 consecutive CVs in 1.0 M $HClO_4$ solution resulted in a slight current decrease revealing instability (Figure S7d).

The rGO, rGO/ZnO, and rGO/PIN/ZnO papers were tested in 1.0 M $HClO_4$ solution for a potential range of −0.1–0.2 V (Figure S8). The highest C_s value in this potential field is obtained for rGO/PIN/ZnO paper as 1.01 mF cm^{-2} but this value is approximately 30 times lower than the C_s value of 31.7 mF cm^{-2} for rGO/PIN paper calculated in the potential range of 0.1–0.7 V (Figure 3). EIS supplies suitable information about electrical resistivity of the samples and it is known that the diameter of the circle obtained in low impedance value is an indicator of the charge transfer resistance (R_{ct}). The R_{ct} values for rGO, rGO/PIN, and rGO/PIN/ZnO paper were calculated as 3537, 682, and 2494 Ω from Nyquist plots of EIS experiments, respectively (Figure S9). The lowest electrical resistivity has been observed for rGO/PIN paper when compared to rGO and rGO/PIN/ZnO papers. Both CV and EIS results indicate that usage of rGO/PIN paper will be useful to gain higher energy storage for an effective supercapattery performance.

CVs of rGO/PIN paper in 1.0 M $HClO_4$ solution between 0.1 V and 0.7 V reveal that peak current density decreases and C_s value increases by the scan rate (Figure 9a, Table S2). The highest C_s value was calculated as 80.16 mF cm^{-2} for 1 mV s^{-1}. Alternatively, C_s values have also been determined by GCD application (Figure 9b). GCD data for rGO/PIN paper in 1.0 M $HClO_4$ solution indicate that C_s value rises by decreasing the current density, resulting the C_s value of 413.9 mF cm^{-2}, energy density of 74.5 W h cm^{-2}, and power density of 2258 W cm^{-2} for current density of 2.2 mA cm^{-2}. Table S3 illustrates the supercapattery performance of previously published studies[27,50–54] but a comparison of rGO/PIN paper with Table S3 is not meaningful due to supercapatteries presented in this table are not fully flexible, the studies are applied in basic (KOH) medium, and the calculations are made by proportion to the mass of the material instead of the electrode surface area.

To determine the charge-discharge stability of rGO/PIN paper, sequential GCD was carried out and it was deduced that the charge-discharge process can be performed in a repeated

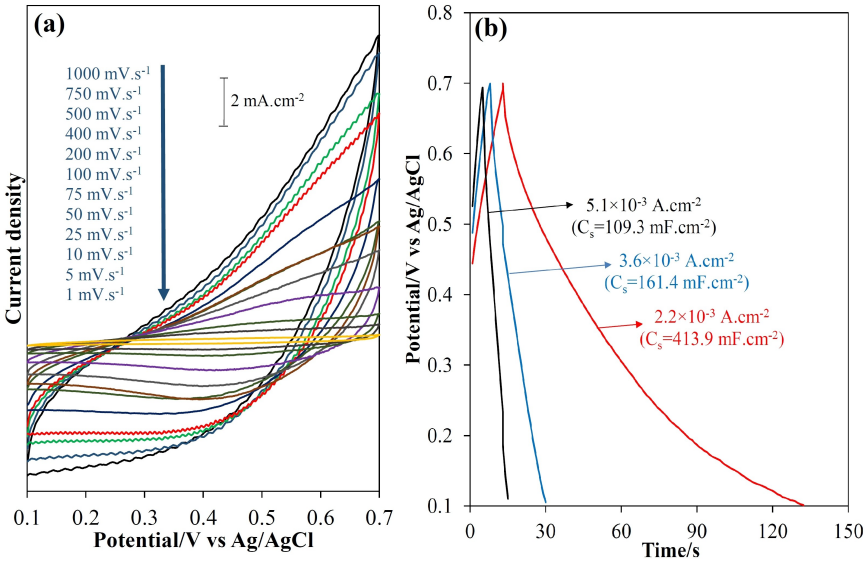

Figure 9. CV (a) and GCD (b) data of rGO/PIN paper in 1.0 M $HClO_4$ solution for different scan rates (a) and current densities (b).

manner until the 550th cycle (Figure S10a). Energy efficieny (EE%) values were also calculated as explained in the supporting information[55] and presented vs scan number in Figure S10b. The EE% of the first scan was 56%, the 50th scan resulted in 65%, and approximately 75% was obtained till the 500th scan. A sudden diminish of EE% to 61% was also observed in Figure S10b, indicating high EE% can be supplied until the 500th scan by this flexible device. The rGO/PIN//rGO supercapacattery system was designed by placing a membrane impregnated with 1.0 M $HClO_4$ solution between rGO and rGO/PIN papers cut in 1.5 cm×2.0 cm dimensions (Figure S10c). To test the energy storage performance of the supercapattery, this system was connected to the power supply and charged at 3 V constant potential for different periods, and then the current density values were read with the amperometer system as shown in Figure S10c. It is observed that the accumulated current density increases with the charging time up to 20 min resulting in current density of approximately 5.7 mA cm^{-2}. Flexible supercapattery production is an important issue for modular and flexible design (Figure S10d). The effect of the flexibility of the prepared rGO/PIN paper on the performance was questioned as shown in Figure S10e. For this experiment, rGO/PIN paper was folded onto itself at different times by 180°, and the C_s value was calculated for each situation. The C_s value increases compared to the initial state up to approximately 150 folds, which can be attributed to the increase in the active surface area with stretching of paper-like material. However, there is a significant decrease of C_s value especially after the 180th fold, indicating the accordance of a weakness at the folded section, which possibly decreases the electrical conductivity at this boundary. It has also been monitored that there is no breakage until the 750th fold, reflecting the highly flexible aspect of the produced rGO/PIN paper.

Conclusions

Flexible and free-standing rGO papers were produced by first mold-casting the GO dispersion and then reducing it with HI treatment. The surface of rGO paper was modified with PIN thin films and ZnO-NPs performing first electropolymerization of indole and then electrodeposition of ZnO-NPs. Thus, the rGO/PIN/ZnO paper structure was prepared and detailed characterizations were carried out using advanced characterization techniques. It was evaluated that the energy storage performance of the rGO/PIN/ZnO paper was approximately 30 times lower than that of the rGO/PIN paper due to the problems with the electrochemical stability of ZnO-NPs at the applied potential region. For this reason, the rGO/PIN paper electrode was elected for supercapacattery design. Based on a current density of 2.2 mA cm^{-2}, the energy density of 74.5 W h cm^{-2} and the power density of 2258 W cm^{-2} were calculated for rGO/PIN paper. For the rGO/PIN//rGO supercapacattery system in an acidic medium, sequential charging/discharging durability was achieved up to 550 cycles with a stable and highly flexible character.

Supporting Information

The supporting information includes calculation of electrode surface area and performance parameters for supercapattery, details of mold-casting procedure, UV-Vis., XRD, STM characterization of GO sheets, CV for electropolymerization of indole, additional XRD, SEM, EIS data of various paper samples, elemental composition of different papers, CVs of paper-like samples in 1.0 M $HClO_4$ solution at various potential window, successive usage stability and flexibility of rGO/PIN//rGO supercapattery, and performance comparison.

Acknowledgements

This study was supported by the Scientific and Technological Research Council of Türkiye (TÜBİTAK) under project no: 121Z206.

Conflict of Interests

The authors declare that they have no known competing financial interests or personal relationships that could have appeared to influence the work reported in this paper.

Data Availability Statement

The data that support the findings of this study are available from the corresponding author upon reasonable request.

Keywords: supercapattery · energy-storage · graphene paper · polyindole · ZnO nanoparticles

[1] E. Azizi, J. Arjomandi, A. Salimi, J. Y. Lee, *Polymer* **2020**, *195*, 122429.
[2] S. Ramesh, H. Yadav, C. Bathula, S. Shinde, A. Sivasamy, H. S. Kim, H. S. Kim, J. H. Kim, *J. Mater. Res. Technol.* **2020**, *9*, 11464.
[3] S. Mondal, S. Aravindan, M. V. Sangarayanan, *Electrochim. Acta* **2019**, *324*, 134875.
[4] N. Bahar, D. Ekinci, *J. Electron. Mater.* **2024**, *53*, 1476.
[5] J. Lu, L. Zhang, C. Xing, G. Jia, Z. Lu, Q. Tian, S. Zhang, J. Lv, *J. Appl. Polym. Sci.* **2022**, *139*, e52801.
[6] S. Jia, X. Zhang, F. Yuan, T. Xia, *ChemistrySelect* **2022**, *7*, e20220298.
[7] T. Fei, T. Ahmad, M. Usman, A. Ahmad, A. Saleem, M. B. Hanif, A. M. Karami, M. S. Javed, B. Akkinepally, C. Xia, *Electrochim. Acta* **2024**, *476*, 143673.
[8] Y. Zhao, Z. Wang, R. Yuan, Y. Lin, J. Yan, J. Zhang, Z. Lu, D. Luo, J. Pietrasik, M. R. Bockstaller, K. Matyjaszewski, *Polymer* **2018**, *137*, 370.
[9] F. Alahmari, S. T. Gunday, A. Iqbal, S. M. Asiri, A. Bozkurt, T. F. Qahtan, E. Cevik, *Int. J. Hydrogen Energy* **2024**, *51*, 357.
[10] G. Liu, J. Liu, K. Xu, L. Wang, S. Xiong, *ChemistrySelect* **2021**, *6*, 6803.
[11] A. Öncü, T. Çetinkaya, H. Akbulut, *Int. J. Hydrogen Energy* **2021**, *46*, 17173.
[12] E. Topçu, *Mater. Res. Bull.* **2020**, *121*, 110629.
[13] E. Erçarıkcı, K. D. Kıranşan, E. Topçu, *IEEE Sens. J.* **2023**, *23*, 7087.
[14] K. D. Kıranşan, E. Topçu, M. Alanyalıoğlu, *J. Appl. Polym. Sci.* **2017**, *134*, 45139.
[15] Z. Aksu, C. H. Şahin, M. Alanyalıoğlu, *Sens. Actuators B* **2022**, *354*, 131198.
[16] Y. Liu, B. Weng, J. M. Razal, Q. Xu, C. Zhao, Y. Hou, S. Seyedin, R. Jalili, G. G. Wallace, J. Chen, *Sci. Rep.* **2015**, *20*, 17045.
[17] W. J. Hyun, E. B. Secor, M. C. Hersam, *MRS Bull.* **2018**, *43*, 730.

[18] J. Liu, S. Song, D. Xue, H. Zhang, *Adv. Mater.* **2012**, *24*, 1089.
[19] C. Klumpner, G. Asher, G. Z. Chen, *IEEE Bucharest Powertech* **2009**, *1–5*, 1104.
[20] B. Ramulu, S. C. Sekhar, G. Nagaraju, J. S. Yu, *Appl. Surf. Sci.* **2020**, *515*, 1460.
[21] M. Hayat, Y. Zhou, M. Z. U. Shah, M. S. Ullah, M. B. Hanif, H. Hou, U. Arif, S. Khan, A. M. Hassan, A. M. Tighezza, M. Sajjad, R. Vadla, *Chemosphere* **2023**, *340*, 139720.
[22] H. Ansarinejad, M. Shabani-Nooshabadi, S. M. Ghoreishi, *Chem. Asian J.* **2021**, *16*, 1258.
[23] Q. Hu, M. Tang, M. He, N. Jiang, C. Xu, D. Lin, Q. Zheng, *J. Power Sources* **2020**, *446*, 227335.
[24] M. Imran, M. W. Iqbal, A. M. Afzal, M. M. Faisal, H. A. Alzahrani, *J. Appl. Electrochem.* **2023**, *53*, 1125.
[25] T. S. Renani, S. M. Khoshfetrat, J. Arjomandi, H. Shi, S. Khazalpour, *J. Mater. Chem. A* **2021**, *9*, 12853.
[26] S. Surendran, R. K. Selvan, *Adv. Mater. Interfaces* **2018**, *5*, 1701056.
[27] S. Surendran, S. Shanmugapriya, S. Shanmugam, L. Vasylechko, R. K. Selvan, *ACS Appl. Energy Mater.* **2018**, *1*, 78.
[28] J. Lin, Z. Zhong, H. Wang, X. Zheng, Y. Wang, J. Qi, J. Cao, W. Fei, Y. Huang, J. Feng, *J. Power Sources* **2018**, *407*, 6.
[29] Q. Zhou, D. Zhu, X. Ma, J. Xu, W. Zhou, F. Zhao, *RSC Adv.* **2016**, *6*, 29840.
[30] M. Tebyetekerwa, S. Yang, S. Peng, Z. Xu, W. Shao, D. Pan, S. Ramakrishna, M. Zhu, *Electrochim. Acta* **2017**, *247*, 400.
[31] H. Mudila, P. Prasher, M. Kumar, A. Kumar, M. G. H. Zaidi, A. Kumar, *Mater. Renewable Sustainable Energy* **2019**, *8*, 9.
[32] I. Marriam, Y. Wang, M. Tebyetekerwa, *Energy Storage Mater.* **2020**, *33*, 336.
[33] K. Parvathi, M. T. Ramesan, *J. Polym. Res.* **2023**, *30*, 55.
[34] J. S. Wellings, N. B. Chaure, S. N. Heavens, I. M. Dharmadasa, *Thin Solid Films* **2008**, *516*, 3893.
[35] A. Öztürk, M. Alanyalıoğlu, *Superlattices Microstruct.* **2016**, *95*, 56.
[36] E. Topçu, K. Dağcı, M. Alanyalıoğlu, *Electroanalysis* **2016**, *28*, 2058.
[37] B. B. Berkes, G. Inzelt, *Electrochim. Acta* **2014**, *122*, 11.
[38] O. Eraldemir, B. Sari, A. Gok, H. I. Unal, *J. Macromol. Sci. Part A* **2008**, *45*, 205.
[39] O. Bayındır, M. Alanyalıoğlu, *ChemistrySelect* **2018**, *3*, 2167.
[40] R. Jia, R. Zhang, L. Yu, X. Kong, S. Bao, M. Tu, X. Liu, B. Xu, *J. Colloid Interface Sci.* **2023**, *630*, 86.
[41] Q. Tan, Z. Kong, X. Guan, L. Y. Zhang, Z. Jiao, H. C. Chen, G. Wu, B. Xu, *J. Colloid Interface Sci.* **2019**, *548*, 233.
[42] R. Wang, K. Lin, F. Jiang, W. Zhou, Z. Wang, Y. Wu, Y. Ding, J. Hou, G. Nie, J. Xu, X. Duan, *Electrochim. Acta* **2019**, *320*, 134641.
[43] Z. J. Cai, Q. Zhang, X. Y. Song, *Electron. Mater. Lett.* **2016**, *12*, 830.
[44] D. Lin-Vien, N. L. Colthup, W. G. Fateley, J. G. Grasselli, *The Handbook of Infrared and Raman Characteristic Frequencies of Organic Molecules*, Academic, New York, NY, USA **1991**.
[45] X. You, S. Maharjan, K. Vinodgopal, J. M. Atkin, *Phys. Chem. Chem. Phys.* **2024**, *26*, 9871.
[46] V. Divya, Y. Jeetika, M. V. Sangaranarayanan, *Mater. Today Proc.* **2020**, *26*, 97.
[47] Ü. Ç. Üst, Ş. B. Demir, K. Dağcı, M. Alanyalıoğlu, *RSC Adv.* **2016**, *6*, 9453.
[48] J.-P. Becker, S. E. Pust, J. Hüpkes, *Electrochim. Acta* **2013**, *112*, 976.
[49] J. Han, W. Qiu, W. Gao, *J. Hazard. Mater.* **2010**, *178*, 115.
[50] J. Iqbal, A. Numan, S. Rafique, R. Jafer, S. Mohamad, K. Ramesh, S. Ramesh, *Electrochim. Acta* **2018**, *278*, 72.
[51] I. Heng, F. W. Low, C. W. Lai, J. C. Juan, N. Amin, S. K. Tiong, *J. Alloys Compd.* **2019**, *796*, 13.
[52] D. J. Tarimo, K. O. Oyedotun, A. A. Mirghni, B. Mutuma, N. F. Sylla, P. Murovhi, N. Manyala, *Int. J. Hydrogen Energy* **2020**, *45*, 33059.
[53] M. Z. Iqbal, M. M. Faisal, M. Sulman, S. R. Ali, M. Alzaid, *J. Electroanal. Chem.* **2020**, *879*, 114812.
[54] J. Iqbal, A. Numan, R. Jafer, S. Bashir, A. Jilani, S. Mohammad, M. Khalid, K. Ramesh, S. Ramesh, *J. Alloys Compd.* **2020**, *821*, 153452.
[55] A. Noori, M. F. El-Kady, M. S. Rahmanifar, R. B. Kaner, M. F. Mousavi, *Chem. Soc. Rev.* **2019**, *48*, 1272.

Manuscript received: February 20, 2024